

Spatio-temporal variations in High-Salinity Shelf Water production in Terra Nova Bay polynya, Antarctica

Seung-Tae Yoon¹, Won Sang Lee¹, Craig Stevens^{2,3}, Stefan Jendersie⁴, SungHyun Nam⁵, Sukyoung Yun¹, Chung Yeon Hwang¹, Gwang Il Jang¹, and Jiyeon Lee¹

¹Korea Polar Research Institute, Yeonsu-gu, Incheon 21990, Republic of Korea

²National Institute of Water and Atmospheric Research, Greta Point, Wellington 6021, New Zealand

³Department of Physics, University of Auckland, Auckland 1142, New Zealand

⁴Victoria University of Wellington, Wellington 6140, New Zealand

⁵Seoul National University, Gwanak-gu, Seoul 08826, Republic of Korea

Correspondence to: Seung-Tae Yoon (styoon@kopri.re.kr)

Abstract.

The formation of High-Salinity Shelf Water (HSSW), which is the major source of Antarctic bottom water (AABW), has been observed in Terra Nova Bay (TNB) in Antarctica. We believe that a description of the spatio-temporal variation of salinity in TNB would help understand the production of HSSW in the region. Hence, the aim of this study is to investigate variations in salinity in the Drygalski Basin (DB) and eastern TNB near Cray Bay on the Ross Sea. For this, we use the moored and profiled hydrographic data, as well as available wind and ice products. We found that the deep salinity in the eastern TNB (~660 m) and DB (~1,200 m) increases each year beginning in September. Significant increases in salinity (> 0.04) were observed in 2016 and 2017. According to velocity data observed at identical depths, the increases in salinity from September were due to the advection of the HSSW from the coastal region of the Nansen ice shelf (NIS). The significant increases in salinity are related to active HSSW formation. In addition, we show that HSSW can be locally formed in the upper layer (< 300 m) of the eastern TNB through convection led by a supply of brine from the surface, which is related to polynya development via winds. Moreover, as compared with historical observations, the salinity of the HSSW has been increasing since 2016 and, in 2018, the salinity was similar to that in early 2000. Observations of fluctuations such as this, which are in contrast to previous freshening, may contribute to the estimation of the properties of recently formed AABW and improve the accuracy of both regional and global climate models.

1 Introduction

The strength of the global meridional overturning circulation is closely associated with the production of Antarctic bottom water (AABW) (Jacobs, 2004; Johnson, 2008; Orsi et al., 1999, 2001), and approximately 25% of the AABW is produced in the Ross Sea (Orsi et al., 2002). In the western Ross Sea, as a result of the strong tidal movement of the Antarctic Slope Front across the shelf break and eddy interaction with the slope's bathymetry, circumpolar deep water (CDW) intrudes the continental shelf to balance High-Salinity Shelf Water (HSSW) off the ice shelf flow (Dinniman 2003; Budillon et al., 2011; St-Laurent et al., 2013; Stewart and Thompson, 2015; Jendersie et al., 2018). Model results suggest that the modified CDW

(MCDW) is advected as far south as Crary Bank, east of Terra Nova Bay (TNB) (Dinniman 2003, Jendersie 2018), although this has not been confirmed by observation. AABW is formed by the mixing of HSSW and CDW or MCDW (Budillon and Spezie, 2000; Budillon et al., 2011; Cincinelli et al., 2008; Gordon et al., 2009). Therefore, HSSW is the major and densest parent water mass of AABW (Budillon and Spezie, 2000; Gordon et al., 2009).

Of the HSSW in the Ross Sea, 33% is produced in Terra Nova Bay polynya (TNBP) (Fusco et al., 2009; Rusciano et al., 2013; Jendersie et al., 2018). TNBP (Fig. 1) is a coastal latent-heat polynya, ~~upon whose surface dense water is formed~~ (Fusco et al., 2002). The Drygalski ice tongue (DIT), which forms the southern boundary of TNBP, blocks ~~sea-ice~~ moving from the south (Stevens et al., 2017). Katabatic winds that blow from the Nansen ice shelf (NIS) take the heat from the polynya, producing sea-ice in TNBP (Fusco et al., 2009; Tamura et al., 2016; Toggweiler and Samuels, 1995), which is responsible for the production of 3–4% of the total sea-ice in Antarctic coastal polynyas (Tamura et al., 2016). The release of ~~salty br~~ is a result of sea-ice growth initiates the formation of HSSW and determines its properties (Fusco et al., 2009; Rusciano et al., 2013).

HSSW is mainly produced during the austral winter (April–October) when TNBP most efficiently produces sea-ice in response to the persistent katabatic winds (van Woert, 1999; Rusciano et al., 2013; Sansiviero et al., 2017; Aulicino et al., 2018). TNBP does open in the austral summer, but HSSW is rarely formed during this period due to the cessation of sea-ice production in the upper layer, along with ice-melting processes (Rusciano et al., 2013). According to historical observations and the results of numerical modelling, the densest HSSW is formed from August to October, during which period the maximum salinity of the HSSW increases to approximately 34.86 (Buffoni et al., 2002; Fusco et al., 2009; Mathiot et al., 2012; Rusciano et al., 2013). Previous studies have suggested that convection, ~~which is preceded by~~ wind-driven mixing is the HSSW formation mechanism (Buffoni et al., 2002; Mathiot et al., 2012). Besides polynya activity, CDW transport in the Ross Sea continental shelf and water masses that flow from the southern part of the DIT have been suggested ~~as the factors that influences changes in~~ HSSW properties (Fusco et al., 2009; Stevens et al., 2017).


The coastal region of the NIS is considered to be the primary location of HSSW formation in TNB, because this region is relatively shallow and katabatic winds blowing from across the NIS first encounter the ocean surface here. For this reason, salinity variations were investigated in the western part of the Drygalski Basin (DB) rather than the eastern TNB (Fusco et al., 2009; Rusciano et al., 2013; Fig. 1). However, the shape of TNBP has varied over time based on MODIS (Moderate-resolution Imaging Spectroradiometer) ice surface temperature imagery (Ciappa et al., 2012; Aulicino et al., 2018), indicating that polynya activity may vary both spatially and temporally. Moreover, as suggested by model results, water masses in the deepest parts of the DB and eastern TNB may interact with water masses in the western Ross Sea via cyclonic circulation over Crary Bank (Jendersie et al., 2018; Fig. 1). In other words, the HSSW accumulates in the deepest parts of the DB and eastern TNB before being predominantly transported north towards the shelf break. As a result, the formation of HSSW in the region may be spatially and temporally modulated by influences from bathymetry, sea ice formation, and winds.

This study uses ship-based *in situ* data collected in the austral summer (December–March) and hydrographic mooring data collected in the DB and eastern TNB during December 2014–March 2018 to explore sub-polynya scale (~10s km) dynamics.

In particular, we seek to answer the following research questions: (1) Does the ~~nature of~~ circulation in TNB influence HSSW production? (2) Are there significant differences between the salinity of the western (nearshore) and eastern (offshore) parts of TNB? and (3) Does wind variability play a role in salinity variation? We ~~use the answers to these questions to pose a~~ sequence of typical mechanistic scales for the polynya.

2 Data and Methods

2.1 Hydrographic measurements

We examined the spatio-temporal variations in HSSW production using the time-series data from mooring  stations in the eastern TNB (DITN) and the deepest depth of the DB (DITD) (~~blue diamond and magenta star, respectively, in Fig. 1~~). The DITN mooring, which supports measurements of temperature, salinity, pressure, and ocean currents at three depths, using SBE37SM (Sea-Bird Scientific, Bellevue, WA, USA), RCM9 (Xylem, Inc., Rye Brook, NY, USA), and Aquadopp (Nortek, Norway) current meters (Fig. 2 and Table 1), has been continuously maintained since December 2014 (Table 1). ~~Data from these devices have been retrieved, downloaded, and maintained, with annual instruments redeployment thereafter. The redeployments are collocated, such that the depths at sensor locations in each observation period were nearly identical during the three year study period (Fig. 2 and Table 1).~~ During the second leg of the DITN, ~~an SBE37SM installed in a deep layer incorrectly recorded the pressure value.~~ Therefore, a nominal sensor depth of 660 m was used to calculate the salinity. ~~In addition, the DITD mooring was deployed for a single year during February 2017–March 2018, which recorded the same variables as the DITN, but operated below 1,200 m (Fig. 2 and Table 1).~~

The temperature and salinity parameters obtained from these moorings were validated and corrected with conductivity-temperature-depth (CTD) casts in the mooring positions before recovery and after the deployment of the DITN and DITD. The magnetic declination ~~was corrected to the current direction~~ and the velocities were averaged monthly to investigate the mean advection speed and direction ~~during each month rather than short-term variabilities in the ocean currents over the course of a month.~~ Current data observed with the RCM9 ~~instrument during the DITN mooring~~ were used for consistency of data analysis, except for the uppermost current data of the third leg of the DITN. Current data from the RCM9 ~~instrument at a depth of 75 m~~ were recorded until August 1, 2017. Thereafter, an Aquadopp current meter was used. Mean differences in the current direction (speed) between observed data from the RCM9 and Aquadopp current meters at each depth were 2°, 3°, and 8° (1.8, 0.2, and –1.2 cm/s), respectively during the third leg of the DITN.

Full-depth CTD profile ~~data~~ measurements were conducted by the icebreaking research vessel IBRV ARAON (Korea Polar Research Institute (KOPRI)) during hydrographic surveys to analyze the water mass properties of TNB. The profiles were recorded using an SBE 911 (Sea-Bird Electronics) ~~along with the CTD~~ with dual temperature and conductivity sensors. The sensors' calibration dates were within seven months of the observation dates. They were processed using standard methods recommended by SBE (Sea-Bird Electronics, Inc., 2014). Surveys on TNB were conducted during December 2014, December 2015, January–February 2017, and March 2018 (Table 1), although profile locations varied annually depending on sea ice and

cruise priorities (Fig. 1). Profiles of horizontal currents (5-m interval) were measured using a lowered acoustic Doppler current profiler (LADCP) instrument attached to the CTD frame. The LADCP data were processed (Thurnherr, 2004) and velocities lower than error velocity were not used in this study. The error velocity indicates uncertainty in the velocity estimated using the LADCP profile (Thurnherr, 2004). In addition, the velocities were de-tided using all ten available tidal components from the CATS2008 (Circum-Antarctica Tidal Simulation model) (Padman et al., 2002). The mean ~~velocity of~~ tidal currents during each survey ~~was~~ 0.9, 1.5, 1.0, and 0.5 cm/s, which were much weaker than the velocities observed from the moorings and LADCP.

To directly compare this study with results from previous studies (Budillon and Spezie, 2000; Budillon et al., 2002; Budillon et al., 2011; Orsi and Wiederwohl, 2009), we used the practical salinity scale, rather than results based on the thermodynamic equation of seawater, i.e., (TEOS)-10 (McDougall and Barker, 2017). Potential densities (σ_θ) over 28 kg/m³ were used as a criterion for the properties of the HSSW, to distinguish the HSSW from TNB ice shelf water (TISW) (Fig. 3). TISW is the product of mixing between meltwater from ice-shelf melting and HSSW (Rusciano et al., 2013).

2.2 Wind and sea-ice data

Hourly wind data (2014–2018) observed at the Automatic Weather System (AWS) Manuela station (Ciappa et al., 2012; Fig. 4a) were used to investigate katabatic winds blowing over TNB. The AWS Manuela station is managed by the Automatic Weather Station Program of the AMRC (Antarctic Meteorological Research Center) at the University of Wisconsin-Madison. A katabatic wind event is defined as having a westerly wind direction of 225–315° and a wind speed of over 25 m/s. The AWS Manuela station is situated such that it is within the pathway of katabatic winds along Reeves Glacier, making it the best option to detect the katabatic winds ~~that blow~~ over TNB (Ciappa et al., 2012; Sansiviero et al., 2017).

The three-hourly 10-m wind and 2-m air-temperature data, provided by the ERA-Interim reanalysis data set (Dee et al., 2011), were also used to identify atmospheric conditions in TNB from January 2014 to March 2018. A grid size of 0.75° × 0.75° was attributed to the data set. Averaged wind at the AWS Manuela station was approximately four times faster than that provided by the ERA-Interim reanalysis data, but its direction was nearly identical with that at the grid located near Manuela (an approximately 6° difference) (Fig. 4a). ERA-Interim is a spatially smoothed product with a grid that is generally too coarse to resolve steep glacial slopes, which may be the reason for the large difference in wind speed compared to the observed data (Fusco et al., 2002; Dee et al., 2011). However, variations in eastward (225° ≤ θ ≤ 315°) wind speed at Manuela had a significant correlation (99% confidence level) with ERA-Interim retrieved values from TNB, including the region near the DITN, from July 2014 to March 2018 (correlation coefficient (r) > 0.70) (Fig. 4b). Eastward winds detected at Manuela station were synchronized with the wind in terms of occurrence and speed variability in all regions of TNB, despite slower offshore wind speeds. In addition, the daily air temperature observed at Manuela also had a significant r value (> 0.90) with that from the ERA-Interim (Fig. 4b).

We also investigated the daily ARTIST (Arctic Radiation and Turbulence Interaction Study) sea-ice algorithm concentration products with a grid spacing of 3.125 km from the Advanced Microwave Scanning Radiometer 2 data set (Spreen et al., 2008).

The selected data period was from July 2014 to March 2018, ~~with a data~~ domain within the McMurdo Sound (Fig. 4a). We applied the same continental masking obtained from recent data and defined regions of sea-ice concentrations below 20% as open water (Parkinson et al., 1999; Zwally et al., 2002). Finally, the topographic data were derived from the International Bathymetric Chart of the Southern Ocean (IBSCO).

3 Results

3.1 Deep salinity variations in TNB

~~Deep salinity observed~~ in a mooring located in the eastern TNB (DITN, blue diamond in Fig. 1) exhibited interannual variations during 2015–2017 (Fig. 5a). ~~Moreover, at approximately 660 m, during a span of three years, the salinity significantly increased from 34.80 to 34.85, despite certain periods where the salinity decreased by 0.01–0.02 (Fig. 5a).~~ The annual cycle of salinity begins to increase from September (Fig. 5a), where the change in salt contents (Fusco et al., 2009) is estimated as 2.84, 7.64, and 5.23 $\mu\text{g salt/m}^3/\text{s}$ (0.007, 0.019, and 0.013 psu/month) from September to October during 2015, 2016, and 2017, respectively. Seawater properties during this period were included in the range of the HSSW (blue dots in Fig. 6). Therefore, the relatively large changes in salt during 2016 and 2017 are an indication of active HSSW formation during the austral winter in TNBP.

Evidence of the past HSSW formation from April to October of 2016 and 2017 was still observed three and five months later, in January 2017 and March 2018, respectively (Fig. 3). The maximum salinity in the HSSW during January–February 2017 (2016/17) and in March 2018 (2017/18) was similar to that of the preceding observations in October of 2016 and 2017, respectively (Fig. 3 and Fig. 5a). The mean salinity in the HSSW ($\sigma_\theta > 28 \text{ kg/m}^3$) was calculated as 34.788 ($\sigma=0.002$), 34.785 (0.005), 34.801 (0.009), and 34.815 (0.016) for each survey. Possible traces of MCDW were rare in the θ -S diagram (small panel in Fig. 3), such that its effect on the changes in deep salinity throughout TNB were limited.

Vertical CTD profiles also had features consistent with the θ -S diagram (Fig. 7). A quasi-homogeneous bottom layer below 800 m represents HSSW formation just before austral winter (Fig. 7). The salinity of this year was relatively high in the 2016/17 and 2017/18 surveys (Fig. 7a; peak salinities of 34.83 and 34.85, respectively). Such a high-salinity water mass can be only formed in TNBP (Orsi and Wiederwohl, 2009). Thus, active HSSW formation in TNBP during the austral winters of 2016 and 2017 increased the salinity of the water at 660 m at the DITN mooring.

The latter two surveys were conducted in the late austral summer (January–February 2017 and March 2018). Therefore, less saline (dense) seawater in the upper parts and a strong salinity (density) gradient between the upper and lower layers were observed (Figs. 7a and 7c). The TISW, characterized by its potential temperatures lower than the freezing point at the surface ($\theta < -1.93^\circ\text{C}$) and a salinity of approximately 34.73 (Budillon and Spezie, 2000), was observed at depths between 300 and 600 m in 2016/17 and 2017/18, but was not observed during December surveys (2014/15 and 2015/16) (Figs. 3 and 7b). Therefore, meltwater outflow from nearby ice shelves may occur in late summer.

Mooring D (a black-filled triangle in Fig. 1) 33km northwest of the DITN, was deployed near the NIS from 1995 to 2007, performing observations of various ocean variables at depths of up to 1,000 m for 13 years. Data from mooring D showed that periods of deep salinity (~ 550 m) increase beginning in July due to HSSW production (Rusciano et al., 2013). However, the timing of the salinity increase at the DITN occurred approximately 1–2 months later than that observed at mooring D. Saline seawater over 34.80 is only formed in TNBP, which is the reason behind the increase in salinity measured in September. According to the current measurements obtained at the same depth (~ 660 m) as the salinity, flows were nearly southward and slower than 4 cm/s (blue arrows in Fig. 5b). Southwestward flows were mainly observed during periods of increased salinity, with episodic detection of southeastward flows (Fig. 5b). The mean current direction was southwestward (191°), with a mean speed of approximately 1.5 cm/s during the August–November period over the three year study period (a blue arrow in Fig. 1). We assumed that the propagation of the HSSW into the eastern TNB for a month along the mean current would result in HSSW movement from 40 km of the DITN in a northern direction. Moreover, the HSSW is formed near the NIS during the austral winter and propagates towards the center of TNB along 800–1,000-m isobaths (Fig. 1) (Rusciano et al., 2013). Thus, we can conclude that the deep salinity in the eastern TNB has increased since September due to the southward advection of HSSW from the center of TNB (75°S , 165°E) near mooring D.

The one-year of moored hydrographic data from the deepest depth of DB (DITD, a magenta star in Fig. 1) also captures the salinity variation feature demonstrated during the third leg of DITN mooring (a magenta line in Fig. 5a). The salinity in the deepest part of TNB also begins to increase from September, and the salt change from September to October 2017 is estimated as $6.66 \mu\text{g salt/m}^3/\text{s}$ (0.017 psu/month) (Fig. 5a). Seawater properties observed from the DITD are also included in the range of HSSW (magenta dots in Figs. 6g–6i). However, northwestward currents are observed at a similar depth of salinity as that from the DITD (1,222 m) during the observation periods (Fig. 5b). The mean direction of the current is northwestward (300°), and its mean speed is approximately 3.0 cm/s during August–November 2017 (a magenta arrow in Fig. 1). The maximum salinity measured at the DITD is larger than that at the DITN (Fig. 5a), so the salinity increase in the DITD is not related to the northwestward HSSW advection from the eastern TNB. Consequently, the current observed from the DITD is considered as a part of the circulation in the deepest parts of DB along the 1,000 m isobath. In other words, HSSW flowing into the DB from the NIS would circulate over the DB, which is being detected at the DITD since September 2017. The circulation in the DB is discussed further in Section 4.2.

3.2 Upper ocean salinity variations in the eastern TNB

Salinity was observed at around 75 and 273 m to investigate the variations in the upper water column of the eastern TNB (Fig. 8a). In contrast to the salinity at 660 m, salinity in the upper parts show a distinct seasonal variation. Salinity at both 75 m and 273 m decreased, while salinity at 75 m decreased to below 34.0 in February of each year (Fig. 8a). Thereafter, the salinity of the two layers start mixing, as the salinity increases (decreases) at 75 (273) m. The salinity of the two layers then increases in tandem from May to October (Fig. 8a). In December, mixing of the two layers ceases and their salinity difference becomes

195 larger again (Fig. 8a). The reduction in mixing is due to changes in buoyancy as a result of ice melting at the surface during the austral summer.

We have noted that the period when these layers are well mixed has become longer over time (Fig. 8a). If we assume that the two layers are mixed when the difference in σ_θ between the two layers is less than 0.1 kg/m^3 ($\sim 0.0005 \text{ kg/m}^2$) (Dong et al., 2008), then early May in 2015, the end of April in 2016, and early April in 2017 are when the upper (at least to 273 m) water column becomes isopycnal (Fig. 8b). From these times until October, salinities at the two depths are characterized by higher correlations than during the entire period. The salinity at 75 m had correlation coefficients of 0.64, 0.58, and 0.62 with the salinity at 273 m during the 1st, 2nd, and 3rd legs (Table 1), respectively. However, for periods in which the salinity at the two depths simultaneously increased, the r values increased to 0.94, 0.88, and 0.93 (Fig. 8a), respectively. In other words, the salinity at the two depths was characterized by the most rapid mixing during March–April 2017 among the three year study period, with the longest co-variation time until October, 2017.

The maximum salinity observed at depths of 75 and 273 m, during September–October also increased from 2015 to 2017 (34.774, 34.804, and 34.849, respectively), which is consistent with the trend of maximum salinity observed at deeper depths (Figs. 5a, 7 and 8a). The HSSW was detected even in the upper parts during the months of August to October in 2016 and 2017 (red and black dots in Figs. 6d–6i). In contrast, HSSW formation was rarely observed from August to October 2015, when the increase in salinity was relatively small compared with that during the same period in 2016 and 2017 (Fig. 5a; red and black dots in 6a–6c).

~~The reasons for the higher increase in salinity in the upper parts may be due to the formation of increasing amounts of dense water via brine rejection at the surface of the eastern TNB or by the advection of more saline water from other regions of TNB. According to current data obtained from the upper parts, westward currents were dominant at the two depths during December 2014–March 2018 (Fig. 8c), with an average current speed (direction) from June to November of 7.4 cm/s (279°, westward) at 75 m and 4.0 cm/s (270°, westward) at 273 m (Fig. 1). These currents are possibly led by density gradients between under the DIT and in TNB or a latitudinal gradient of sea-surface height near the DIT. These phenomena are confined to coastal regions due to the existence of the DIT (Fig. 1 and Section 1). However, based on our observations, only the upper water columns of the DITN appear to be affected by seawater from the eastern part of TNB during periods of increased upper level salinity. As identified in previous studies, water masses farther away TNB are less saline due to mixing with the CDW or the intrusion of MCDW into the western Ross Sea (Orsi and Wiederwohl, 2009; Fusco et al., 2009; Budillon et al., 2011).~~

Thus, salinity increases in the upper layers are related to local brine supplied by sea-ice formation near the DITN region, rather than the advection of saline water from the western Ross Sea. As a result, salinity (density) variations in the upper layers exhibit dense water formation in the polynya via convection led by a supply of brine from the surface as suggested by modelling studies on TNBP (Fig. 8a; Buffoni et al., 2002; Mathiot et al., 2012). We observed the HSSW in the upper layers during the months from August to October of 2016 and 2017 (Fig. 6d–6i, and 8a), which indicates that the HSSW can be formed through convective processes in the eastern TNB. In addition, mixing of the upper layers in the eastern TNB was observed before

convection, which implies that winds drive mixing as well as polynya development. We discuss ~~to~~ this point further in Section 3.4.

3.3 Types of HSSW

We found that the ~~deep~~ salinity began to increase in September, and the HSSW was detected in the upper parts of the DITN during August–October (Fig. 5a and 6). Based on numerical modelling, a water column in TNB can be mixed to a depth of 750 m, forming an HSSW layer from the surface to this depth (Buffoni et al., 2002; Mathiot et al., 2012). In other words, the increase in the deep salinity (i.e., at 660 and 1,208 m) observed in 2016 and 2017 may have been partly induced by local HSSW formation combined with HSSW advection from the center of TNB. However, the salinity time-series at 660 m had a poor correlation with salinity variations in the upper parts of the DITN during September–October in 2016 and 2017 ($r < 0.30$). The salinity at 660 m was **a little higher** than that observed in the upper water column (Figs. 6 and 8a). This indicates that the mixed layer does not extend to 660 m in the eastern TNB. The higher salinity in the deep layer derives from the other regions in TNB and, not the surface of the DITN. Thus, in this case, the HSSW formed in the eastern TNB must be distinguished from that produced in the coastal region of the NIS. **Its** involvement in the upper layers of TNB or its influence on the eastern TNB are equally interesting research topics but **these** types of HSSW are difficult to investigate with the observational data used in this study.

3.4 Role of wind in TNBP

The wind in TNB is primarily westerly, which on average, creates an L-shaped polynya along the NIS and DIT, as shown by the contour line that represents a sea-ice concentration of 50% in Fig. 4a. Westerly winds measured at Manuela effectively open TNBP during the austral winters of the three year study period (Fig. 9). The ~~r value~~ between the daily wind speed (blue line in Fig. 9) and the percentage of open water (sky blue bars in Fig. 9) was 0.46 across a seven-month period (April–October, red dashed boxes in Fig. 9) during the three year period (2015–2017), which is significant at a 99% confidence level. In the austral winter during each year, the r value was 0.49, 0.50, and 0.37, where all values were significant at a 99% confidence level. The period from the end of June to July 2017, when open water did not significantly expand despite strong winds, affected the estimation of the lowest r value during the austral winter of 2017. The weak response of the polynya to these winds appears to be associated with a blocking effect of sea-ice in the offshore region (Tamura et al., 2016).

Previous studies have suggested that HSSW formation near mooring D is more dependent on the duration of a single katabatic wind event, than on its frequency during April–October (Rusciano et al., 2013). Based on the hydrographic surveys of TNB, there was more active formation of the HSSW in 2016 and 2017 than in 2014 and 2015. Therefore, **deep salinity** was increased due to HSSW advection from mooring D during late 2016 and 2017. This is consistent with wind observations at Manuela station. Among the three years, katabatic wind events most frequently occurred from April to October 2017 (210 events). The mean duration of a single katabatic wind event during these seven months in 2015, 2016, and 2017 was **6.5, 7.0, and 7.7 hours** respectively. Moreover, the average length of time for which the polynya was open (i.e., > 20% open water) during the same

260 periods was 5.8 (2015), 6.7 (2016), and 7.7 days (2017), respectively. These results suggest that, during the three year study period, HSSW formation was the most active near the NIS during the 2017 austral winter.

In addition, from September to October of 2016 and 2017, the upper layers of the eastern TNB also experienced HSSW production via convective processes after the development of a mixed layer. This indicates that katabatic winds — considered as pivotal to the development of a polynya (Fig. 9) and HSSW formation near the NIS (Rusciano et al., 2013) — generate wind-driven mixing and induce ~~the convection by a supply of brine related to polynya development~~ in the eastern TNB. Wind-driven mixing mainly occurs from March to May in the upper layers of the eastern TNB (Figs. 8a, and 8b), such that the mean wind speed (number of katabatic wind events) from March to May during 2015, 2016, and 2017 was calculated as 18.6, 20.2, and 21.0 m/s (74, 85, and 96), respectively. These wind statistics represent that wind-driven mixing was the strongest between March and May 2017 among the three years, which is consistent with the ~~fastest mixing at two depths~~ observed during the same period in the upper layers of the eastern TNB (Fig. 8a, and 8b).

When the salinity in the upper layers of the eastern TNB were predominantly increased through the convection led by a brine supply from the surface (June–September) (Fig. 8a), the total magnitude of the increase in salinity during the katabatic wind events was the largest in 2017 at both 75 (0.082, 0.118, and 0.120 in each year), and 273 m (0.065, 0.050, and 0.142 in each year) among the three years. The salinity time-series contains the short-term fluctuation (Fig. 8a) induced by tidal motions and ocean currents, such that the magnitude of the change in the salinity was calculated after applying a 160 hour (~ 7 days) low-pass filter to the time-series using the 6th order Butterworth filter. Increases in the salinity related with katabatic wind events accounted for over 50% (54% at 75 m and 76% at 273 m) of the total salinity increase from June to September in 2017. In other words, ~~the convection promoted by the most brine supply~~ during the katabatic wind events in 2017 contributed to a larger increase in salinity in the upper layers of the eastern TNB and local HSSW formation.

280 4 Discussion

Despite being a small, confined polynya, TNBP generates a substantial proportion of the global AABW. Understanding the supply of HSSW, and ultimately AABW, requires a focus on small scale processes from a regional perspective. Here, we investigate HSSW behaviours in TNB ~~are investigated with~~ the spatio-temporal variations in salinity observed in the eastern TNB and DB.

285 4.1 Present data in the context of previous analyses

Data from mooring D (Fig. 1) in TNBP show seasonal variation in the stratification of the water column and interannual variation in the HSSW properties, which are closely associated with polynya activity (Rusciano et al., 2013). This proves that HSSW production occurs during the austral winter, and ~~a series of katabatic wind events in a certain period of time during the austral winter controls~~ the properties of the HSSW. Data gathered for this study have revealed that the HSSW can also form at the surface of the eastern TNB via an identical polynya process as that involved in vigorous HSSW formation near the NIS.

In addition, we found that large increases in salinity (> 0.04) observed in the deepest part of the DB and eastern TNB were due to HSSW advection ~~and not a sinking~~ HSSW directly from the surface at the mooring locations. The HSSW formed near the NIS arrives at these depths within a few months. Thus, the HSSW is evenly distributed over TNB during the austral summer. In other words, the average salinity of the HSSW in the eastern part at 164.5°E (34.802) shows no difference from that in the western part at 164.5°E (34.802) during the CTD observation periods. According to vertical sections of salinity from the 2017/18 survey, salinity in the deep layer (> 600 m) was nearly identical between the western and eastern part of TNB (Fig. 10a), with a sufficiently distributed salinity over 34.80 at greater depths (> 800 m) of the DB (Fig. 10b). As a result, the DITN, DITD, and four hydrographic surveys, along with previous data from mooring D, reveal spatio-temporal variations in HSSW production and ~~movement~~ in TNBP.

4.2 Circulations in TNBP

For the austral summer (December–March), westward currents flowing along the DIT and northward currents along the NIS were observed based on the de-tided LADCP current data averaged over a depth range of 400 – 700 m (Fig. 11a). The currents resemble a cyclonic pattern together with the southeastward currents in the northeastern TNB, despite southward currents that flow toward the DIT along 800 – 1000 m isobaths, as well as at the center of the DB (Fig. 11a). However, southeastward currents that cross over from the NIS to the DIT were rarely observed in TNBP. The direction of the ocean current at 660 m in the DITN was stable during December 2014–March 2018 (Figs. 5b and 8c). Therefore, if we assume that the circulation pattern was maintained throughout the year, then the HSSW formed near the NIS may circulate clockwise, arriving in the DITN around September and induced an increase in the salinity, rather than directly propagating southeastward to the DITN. Furthermore, the ~~wind-forcing-driven~~ cyclonic gyre in the upper layer of TNBP (van Woert et al., 2001) may induce an upwelling in the center of TNB, which hinders the development of horizontal flows in the central region of the gyre. For example, the upwelling feature is visible in the vertical sections of the 2017/18 survey as upward-bending isopycnals in the upper layers (> 400 m) of the mid-point of TNB (Fig. 10b).

The bottom currents in the DB flow under the influence of gravity (Jendersie et al., 2018). However, it is still unclear how the HSSW ~~flowing at greater depths~~ ~~is~~ circulated around the DB. The LADCP data for December–March can be an indication of circulation in the DB region ($> 1,000$ m) because the current direction at the DITD exhibits little seasonal variation (Fig. 5b). The southwestward currents appear in the northeastern part of the DB, while the northwestward and northeastward currents appear in the southern and western region of the DB, according to the currents averaged from 900 m to the seafloor during the austral summer (Fig. 11b). The currents resemble a cyclonic circulation confined in the DB, which is different from the upper ocean cyclonic gyre in TNB (van Woert et al., 2001). **In other words,** the HSSW propagating into the DB from the NIS circulated cyclonically in this region and can be detected at the DITD from September. Together with the Ross Ice Shelf polynya, the DB region is regarded as an outflow path of the HSSW towards the Ross Sea. Therefore, the circulation pattern in this region also requires investigation by acquiring more *in situ* ocean current data and ocean circulation model developments.

4.3 TNBP mechanical scales

Considering the range and scale of the physical processes active in TNBP is useful. HSSW produced near the NIS spreads horizontally into the eastern TNB (~35 km) and DB (~25 km), at current speeds lower than 5 cm/s in less than 2 months (from July to September) (Figs. 1, 5, and 8; Rusciano et al., 2013). Simultaneously, the HSSW sinks cyclically to the greatest depths of the DB (~1,200 m) (Fig. 5). If we assume that the circulation in TNBP has a radius of 25 km (approximately one longitudinal degree) (Fig. 11), then we can deduce that the HSSW circulates cyclonically about 80 from the NIS to the eastern parts of TNB, which takes about one month at a current speed of 3 cm/s. In this case, the sinking process should take less than one month at an average velocity of 0.05–0.07 cm/s. The vertical velocity may be at a scale of about 10^{-2} that of the horizontal velocities in TNBP, which is regarded as a reasonable result for the ocean (van Haren, 2018). TNBP usually forms as an L-shape, similar to a model-derived polynya (Sansiviero et al., 2017; Fig. 4a). This indicates that the open water is predominantly formed along the coasts near NIS (DIT) for approximately 75 (85) km. The average area for polynya activity is approximately 1,600 km², based on assuming that the width of the open water is 10 km from the coast using the 40% sea-ice concentration contour line (Fig. 4a). This accounts for about 5% of the sea ice production area in the Ross Ice Shelf polynya (Cheng et al., 2017). In the eastern TNB, wind-driven mixing from the surface to a depth of 273 m occurs within 3 months in March to May). The homogenous mixed layer is maintained above 273 m during the austral winter by persistent, strong winds, and the water column is stratified again from December. The opening of TNBP by westerly winds that blow from across the NIS occur over the span of a day. During this time, the percentage of the open water can vary by up to $\pm 40\%$. The mean duration of the polynya opening is about 6.7 s during the austral winter in the analysis period. Salinity at both 75 and 273 m increased together from June or July (i.e., after the development of a mixed layer from the surface to a depth of 273 m), which indicates that brine rejection by sea-ice formation begins during this period.

4.4 Quantification of sea-ice production

The precise quantification of sea-ice production and brine formation in the polynya region is required for an in-depth understanding of dense-water formation processes. However, current data for the brine supply from sea-ice formation in the polynya provided insufficient constraints. According to previous results obtained using the ERA-Interim data set (Tamura et al., 2016), the estimated amounts of sea-ice production in TNBP had a high correlation ($r = 0.96$) with a thin ice area (< 0.2 m), but exhibited a poor correlation ($r < 0.3$) with offshore winds from the NIS and air temperature in TNB (see Table 1 in Tamura et al., 2016). This implies that the reanalysis data set did not reflect the air-sea heat exchange induced by winds that blow over TNBP or the differences in temperature between the ocean and atmosphere in TNBP. HSSW production was estimated using the changes in the heat flux averaged over TNB (Fusco et al., 2009). In near future, however, spatio-temporal variabilities in surface heat flux should also be investigated to determine the spatial variations in polynya functions throughout TNB over time. Therefore, *in situ* data should be continuously collected to validate reanalysis data sets and suggest spatial and temporal relationships among wind speed, heat flux, sea-ice production, and the brine effect in TNBP. In addition, algorithms

should be developed to accurately process satellite data or new satellite observations to extract data on small-scale ice formations such as frazil ice.

5 Conclusions

This study investigated the spatial patterns and temporal changes in HSSW formation in TNBP during the period December 2014–March 2018 using a large, collaboratively produced data set. We found that HSSW formed near the NIS flows along cyclonic pattern currents in the deeper parts of TNBP and influences the eastern TNB, with the greatest depth in the DB from September (Fig. 12). As a result, the timing of the increase in salinity is about two months later in the eastern (offshore) parts of TNB than in the western (nearshore) parts. Moreover, we found that katabatic winds that blow from across the NIS drive general salinity increases and even HSSW formation by promoting convection with more brine supply in the upper parts of eastern TNB (Fig. 12). These findings answer the three research questions proposed in Section 1, complementing the results of previous studies on HSSW formation in TNBP.

Large-scale freshening of AABW sources (including HSSW) has been reported in the Ross Sea and TNB in recent decades (Jacobs et al., 2002; Fusco et al., 2009; Jacobs and Giulivi, 2010). The intensification of Southern Hemisphere westerlies (in associated with a more positive phase of the Southern Annular Mode) was proposed as a possible driver of ice-sheet melting and corresponding seawater freshening upstream of the Ross Sea, because these processes induce an upwelling of warm water in the Amundsen and Bellingshausen Seas (Jacobs and Giulivi, 2010). In addition, variability in sea-ice production is expected to play a large role in HSSW formation (Jacobs and Giulivi, 2010).

The averaged salinity in a 10-m layer at a depth of 900-m depth shows larger values (> 0.025) in the 2016/17 and 2017/18 surveys than those in the 2014/15 and 2015/16 surveys (Table 1). In other words, the salinity of the HSSW formed in TNBP is increasing again, and its value corresponds to those observed in the early 2000 (Fusco et al., 2009). The HSSW formed in TNB can flow off the shelf break along Victoria Land (Cincinelli et al., 2008; Jendersie et al., 2018), which also contributes to the volumes or properties of AABW in the western Ross Sea. However, the response of overturning circulations in the Southern Ocean to regional anomalies in buoyancy forcing have not been investigated (Rintoul, 2018).

Lastly, here, the potential temperature and practical salinity were used to ensure consistency between our results and previous studies. In future studies, however, the HSSW in TNB needs to be re-defined with a conservative temperature and absolute salinity (TEOS-10) to reduce uncertainties in the long-term trend of HSSW properties, as well as to find a quantitative relationship with water mass properties in other regions.

Data Availability

The observational data used in this study are held at the Korea Polar Data Center (<https://kpdc.kopri.re.kr>) and metadata DOIs are as follows: <https://dx.doi.org/doi:10.22663/KOPRI-KPDC-00001062.1>, <https://dx.doi.org/doi:10.22663/KOPRI-KPDC-00000601.1>, <https://dx.doi.org/doi:10.22663/KOPRI-KPDC-00001063.1>, and <https://dx.doi.org/doi:10.22663/KOPRI->

KPDC-00000895.1 for CTD data; <https://dx.doi.org/doi:10.22663/KOPRI-KPDC-00000895.1>,
<https://dx.doi.org/doi:10.22663/KOPRI-KPDC-00001061.1>, <https://dx.doi.org/doi:10.22663/KOPRI-KPDC-00001065.1>, and
390 <https://dx.doi.org/doi:10.22663/KOPRI-KPDC-00000896.1> for LADCP data; <https://dx.doi.org/doi:10.22663/KOPRI-KPDC-00001060.1>,
<https://dx.doi.org/doi:10.22663/KOPRI-KPDC-00000749.1>, and <https://dx.doi.org/doi:10.22663/KOPRI-KPDC-00000898.1> for DITN data; and <https://dx.doi.org/doi:10.22663/KOPRI-KPDC-00000906.1> for DITD data. The wind
data at the AWS Manuela station and sea ice concentration data used in this manuscript are obtained from
<http://amrc.ssec.wisc.edu/aws/api/form.html>, and https://seaice.uni-bremen.de/data/amsr2/asi_daygrid_swath/s3125/,
respectively. The daily ERA-Interim reanalysis dataset is downloaded from [https://apps.ecmwf.int/datasets/data/interim-full-](https://apps.ecmwf.int/datasets/data/interim-full-daily/levtype=sfc/)
395 [daily/levtype=sfc/](https://apps.ecmwf.int/datasets/data/interim-full-daily/levtype=sfc/).

Author contribution

WSL and CS conceived and designed the experiments. STY, WSL, CS, SY, CYH, GIJ, and JL collected the observational data in TNBP, and STY and CS processed them. STY led the analysis with contributions from WSL, CS, SJ, SN, and CYH. STY wrote the paper.

400 ***Competing Interests***

The authors declare no conflicts of interest.

Acknowledgements

This study was sponsored by a research grant from the Korean Ministry of Oceans and Fisheries (KIMST20190361; PM19020), the New Zealand Antarctic Research Institute, NZ Ministry of Business, Innovation and Employment, and the New Zealand
405 National Institute of Water and Atmospheric Research (NIWA) (NZARI1401). We thank Gary Wilson, Christopher J. Zappa, Pierre Dutrieux, Brett Grant, Fiona Elliott and Alex Forrest for their support of this study through data collection and analysis as well as contributions to earlier versions of the paper.

References

Aulicino, G., Sansiviero, M., Paul, S., Cesarano, C., Fusco, G., Wadhams, P. and Budillon, G.: A new approach for monitoring
410 the Terra Nova Bay polynya through MODIS Ice Surface Temperature Imagery and its validation during 2010 and 2011 winter seasons, *Remote Sens.*, 10, 366, <https://doi.org/10.3390/rs10030366>, 2018.

Budillon, G. and Spezie, G.: Thermohaline structure and variability in the Terra Nova Bay polynya, Ross Sea, *Antarct. Sci.*, 12(4), 493–508, <http://doi.org/10.1017/S0954102000000572>, 2000.

Budillon, G., Cordero, S. G. and Salusti, E.: On the dense water spreading off the Ross Sea Shelf (Southern Ocean), *J. Mar.*
415 *Syst.*, 35, 207–227, [https://doi.org/10.1016/S0924-7963\(02\)00082-9](https://doi.org/10.1016/S0924-7963(02)00082-9), 2002.

- Budillon, G., Castagno, P., Aliani, S., Spezie, G. and Padman, L.: Thermohaline variability and Antarctic bottom water formation at the Ross Sea shelf break, *Deep-Sea Res. Part I*, 58, 1002–1018, <http://doi.org/10.1016/j.dsr.2011.07.002>, 2011.
- Buffoni, G., Cappelletti, A. and Picco, P.: An investigation of thermohaline circulation in the Terra Nova Bay polynya, *Antarct. Sci.*, 14(1), 83–92, <http://dx.doi.org/10.1017/S0954102002000615>, 2002.
- 420 Cheng, Z., Pang, X., Zhao, X. and Tan, C.: Spatio-temporal variability and model parameter sensitivity analysis of ice production in Ross Ice Shelf polynya from 2003 to 2015, *Remote Sens.*, 9, 934, 1–20, <https://doi.org/10.3390/rs9090934>, 2017.
- Ciappa, A., Pietranera, L. and Budillon, G.: Observations of the Terra Nova Bay (Antarctica) polynya by MODIS ice surface temperature imagery from 2005 to 2010, *Remote Sens. Environ.*, 119, 158–172, <http://doi.org/10.1016/j.rse.2011.12.017>, 2012.
- Cincinelli, A., Martellini, T., Bittoni, L., Russo, A., Gambaro, A. and Lepri, L.: Natural and anthropogenic hydrocarbons in the water column of the Ross Sea (Antarctica), *J. Mar. Syst.*, 73, 208–220, <https://doi.org/10.1016/j.jmarsys.2007.10.010>, 2008.
- 425 Dee, D. P., Uppala, S. M., Simmons, A. J., Berrisford, P., Poli, P., Kobayashi, S., Andrae, U., Balmaseda, M. A., Balsamo, G., Bauer, P., Bechtold, P., Beljaars, A. C. M., Berg, L. V., Bidlot, J., Bormann, N., Delso, C., Dragani, R., Fuentes, M., Geer, A. J., Haimberger, L., Healy, S. B., Hersbach, H., Holm, E. V., Isaksen, I., Kallberg, P., Kohler, M., Matricardi, M., McNally, A. P., Monge-Sanz, B. M., Morcrette, J. J., Park, B. K., Peubey, C., Rosnay, P., Tavolato, C., Thepaut, J. N. and Vitart, F.: The
- 430 ERA-Interim reanalysis: configuration and performance of the data assimilation system, *Q. J. R. Meteorol. Soc.*, 137, 553–597, <https://doi.org/10.1002/qj.828>, 2011.
- Dinniman, M. S., Klinck, J. M. and Smith, W. O. Jr.: Cross-shelf exchange in a model of the Ross Sea circulation and biogeochemistry, *Deep-Sea Res. Part II*, 50, 3103–3120, <https://doi.org/10.1016/j.dsr2.2003.07.011>, 2003.
- Dong, S., Sprintall, J., Gille, S. T. and Talley, L.: Southern Ocean mixed-layer depth from Argo float profiles, *J. Geophys. Res.*, 113, C06013, <http://doi.org/10.1029/2006JC004051>, 2008.
- 435 Fusco, G., Budillon, G. and Spezie, G.: Surface heat fluxes and thermohaline variability in the Ross Sea and in Terra Nova Bay polynya, *Cont. Shelf Res.*, 29, 1887–1895, <http://dx.doi.org/10.1016/j.csr.2009.07.006>, 2009.
- Fusco, G., Flocco, D., Budillon, G., Spezie, G. and Zambianchi, E.: Dynamics and variability of Terra Nova Bay polynya, *Mar. Ecol.*, 23, 201–209, <https://doi.org/10.1111/j.1439-0485.2002.tb00019.x>, 2002.
- 440 Gordon, A. L., Orsi, A. H., Muench, R., Huber, B. A., Zambianchi, E. and Visbeck, M.: Western Ross Sea continental slope gravity currents, *Deep-Sea Res. Part II*, 56, 796–817, <http://doi.org/10.1016/j.dsr2.2008.10.037>, 2009.
- Jacobs, S. S.: Bottom water production and its links with the thermohaline circulation, *Antarct. Sci.*, 16, 427–437, <https://doi.org/10.1017/S095410200400224X>, 2004.
- Jacobs, S. S. and Giulivi, C. F.: Large Multidecadal salinity trends near the Pacific-Antarctic Continental margin, *J. Clim.*, 23, 4508–4524, <https://dx.doi.org/10.1175/2010JCLI3284.1>, 2010.
- 445 Jacobs, S. S., Giulivi, C. F., and Mele, P. A.: Freshening of the Ross Sea during the late 20th century, *Science*, 297, 386–388, <https://dx.doi.org/10.1126/science.1069574>, 2002
- Jendersie, S., Williams, M. J. M., Langhorne, P. J. and Robertson, R.: The density-driven winter intensification of the Ross Sea circulation, *J. Geophys. Res. Oceans*, 123, 1–23, <https://doi.org/10.1029/2018JC013965>, 2018.

450 Johnson, G. C.: Quantifying Antarctic Bottom Water and North Atlantic Deep Water volumes, *J. Geophys. Res. Oceans*, 113, C05027, <https://doi.org/10.1029/2007JC004477>, 2008.

Mathiot, P., Jourdain, N. C., Barnier, B., Gallee, H., Molines, J. M., Sommer, J. L. and Penduff, T.: Sensitivity of coastal polynyas and high-salinity shelf water production in the Ross Sea, Antarctica, to the atmospheric forcing, *Ocean Dyn.*, 62, 701–723, <http://dx.doi.org/10.1007/s10236-012-0531-y>, 2012.

455 McDougall, T. J. and Barker, P. M.: Getting started with TEOS-10 and the Gibbs Seawater (GSW) Oceanographic Toolbox – version 3.06.3, 28pp., SCOR/IAPSO WG127, ISBN 978-0-646-55621-5, 2017.

Orsi, A. H., Jacobs, S. S., Gordon, A. L. and Visbeck, M.: Cooling and ventilating the Abyssal Ocean, *Geophys. Res. Lett.*, 28(15), 2923–2926, <https://doi.org/10.1029/2001GL012830>, 2001.

Orsi, A. H., Johnson, G. C. and Bullister, J. L.: Circulation, mixing, and production of Antarctic Bottom Water, *Prog. Oceanogr.*, 43, 55–109, [https://doi.org/10.1016/S0079-6611\(99\)00004-X](https://doi.org/10.1016/S0079-6611(99)00004-X), 1999.

460 Orsi, A. H., Smethie Jr., W. M. and Bullister, J. L.: On the total input of Antarctic waters to the deep ocean: a preliminary estimate from chlorofluorocarbon measurements, *J. Geophys. Res. Oceans*, 107(C8), 3122, <https://doi.org/10.1029/2001JC000976>, 2002.

Orsi, A. H. and Wiederwohl, C. L.: A recount of Ross Sea waters, *Deep-Sea Res. Part II*, 56, 778–795, <http://doi.org/10.1016/j.dsr2.2008.10.033>, 2009.

465 Padman, L., Fricker, H. A., Coleman, R., Howard, S. and Erofeeva, L.: A new tide model for the Antarctic Ice shelves and Seas, *Ann. Glaciol.*, 34, 1–14, <https://doi.org/10.3189/172756402781817752>, 2002.

Parkinson, C. L., Cavalieri, D. J., Gloersen, P., Zwally, H. J. and Comiso, J. C.: Arctic sea ice extents, areas, and trends, 1978–1996, *J. Geophys. Res. Oceans*, 104(C9), 20,837–20,856, <https://doi.org/10.1029/1999JC900082>, 1999.

470 Rintoul, S. R.: The global influence of localized dynamics in the Southern Ocean, *Nature*, 558, 209–218, <http://doi.org/10.1038/s41586-018-0182-3>, 2018.

Rusciano, E., Budillon, G., Fusco, G., and Spezie, G.: Evidence of atmosphere–sea ice–ocean coupling in the Terra Nova Bay polynya (Ross Sea–Antarctica), *Cont. Shelf Res.*, 61–62, 112–124, <http://dx.doi.org/10.1016/j.csr.2013.04.002>, 2013.

Sansiviero, M., Maqueda, M. A. M., Fusco, G., Aulicino, G., Flocco, D. and Budillon, G.: Modelling sea ice formation in the Terra Nova Bay polynya, *J. Mar. Syst.*, 166, 4–25, <http://dx.doi.org/10.1016/j.jmarsys.2016.06.013>, 2017.

475 Sea-Bird Electronics, Inc.: Seasoftware V2: SBE data processing (User’s Manual, pp. 1–174). Bellevue, Washington, USA, 2014.

Spreen, G., Kaleschke, L. and Heygster, G.: Sea ice remote sensing using AMSR-E 89 GHz channels, *J. Geophys. Res. Oceans*, 113, C02S03, <https://doi.org/10.1029/2005JC003384>, 2008.

Stevens, C., Lee, W. S., Fusco, G., Yun, S., Grant, B., Robinson, N. and Hwang, C. Y.: The influence of the Drygalski Ice Tongue on the local ocean, *Ann. Glaciol.*, 58(74), 51–59, <https://doi.org/10.1017/aog.2017.4>, 2017.

480 Stewart, A. L. and Thompson, A. F.: Eddy-mediated transport of warm Circumpolar Deep Water across the Antarctic shelf break, *Geophys. Res. Lett.*, 42, 432–440, <https://doi.org/10.1002/2014GL062281>, 2015.

- St-Laurent, P. Klinck, J. M. and Dinniman, M. S.: On the role of coastal troughs in the circulation of warm Circumpolar Deep Water on Antarctic shelves, *J. Phys. Oceanogr.*, 43(1), 51–64, <https://doi.org/10.1175/JPO-D-11-0237.1>, 2013.
- 485 Tamura, T., Ohshima, K. I., Fraser, A. D. and Williams, G. D.: Sea ice production variability in Antarctic coastal polynyas, *J. Geophys. Res. Oceans*, 121, 2967–2979, <https://doi.org/10.1002/2015JC011537>, 2016.
- Toggweiler, J. R. and Samuels, B.: Effect of sea ice on the salinity of Antarctic bottom waters, *J. of Phys. Oceanogr.*, 25, 1980–1997, [https://doi.org/10.1175/1520-0485\(1995\)025<1980:EOSIOT>2.0.CO;2](https://doi.org/10.1175/1520-0485(1995)025<1980:EOSIOT>2.0.CO;2), 1995.
- Thurnherr, A. M.: How to Process LADCP Data with the LDEO Software. New York: Columbia University.
 490 ftp://ftp.ldeo.columbia.edu/pub/LADCP/HOWTO/LDEO_IX.pdf, 2014.
- van Haren, H.: High-resolution observations of internal wave turbulence in the deep ocean, *The ocean in motion: Circulation, Waves, Polar oceanography*, edited by: Velarde M. G., Tarakanov, R. Y., and Marchenko, A. V., Springer, Gewerbestrasse, Cham, Switzerland, 127–146, 2018.
- van Woert, M. L.: Wintertime dynamics of the Terra Nova Bay polynya, *J. Geophys. Res. Oceans*, 104, C4, 7753–7769,
 495 <https://doi.org/10.1029/1999JC900003>, 1999.
- van Woert, M. L., Meier, W. N., Zou, C.-Z., Archer, A., Pellegrini, A., Grigioni, P. and Bertola, C.: Satellite observations of upper-ocean currents in Terra Nova Bay, Antarctica. *Ann. Glaciol.*, 22, 407–412, <https://doi.org/10.3189/172756401781818879>, 2001.
- Zwally, H. J., Comiso, J. C., Parkinson, C. L., Cavalieri, D. J. and Gloersen, P.: Variability of Antarctic sea ice 1979–1998. *J.*
 500 *Geophys. Res. Oceans*, 107(C5), 3041, 9-1–9-19, <https://doi.org/10.1029/2000JC00007>, 2002.

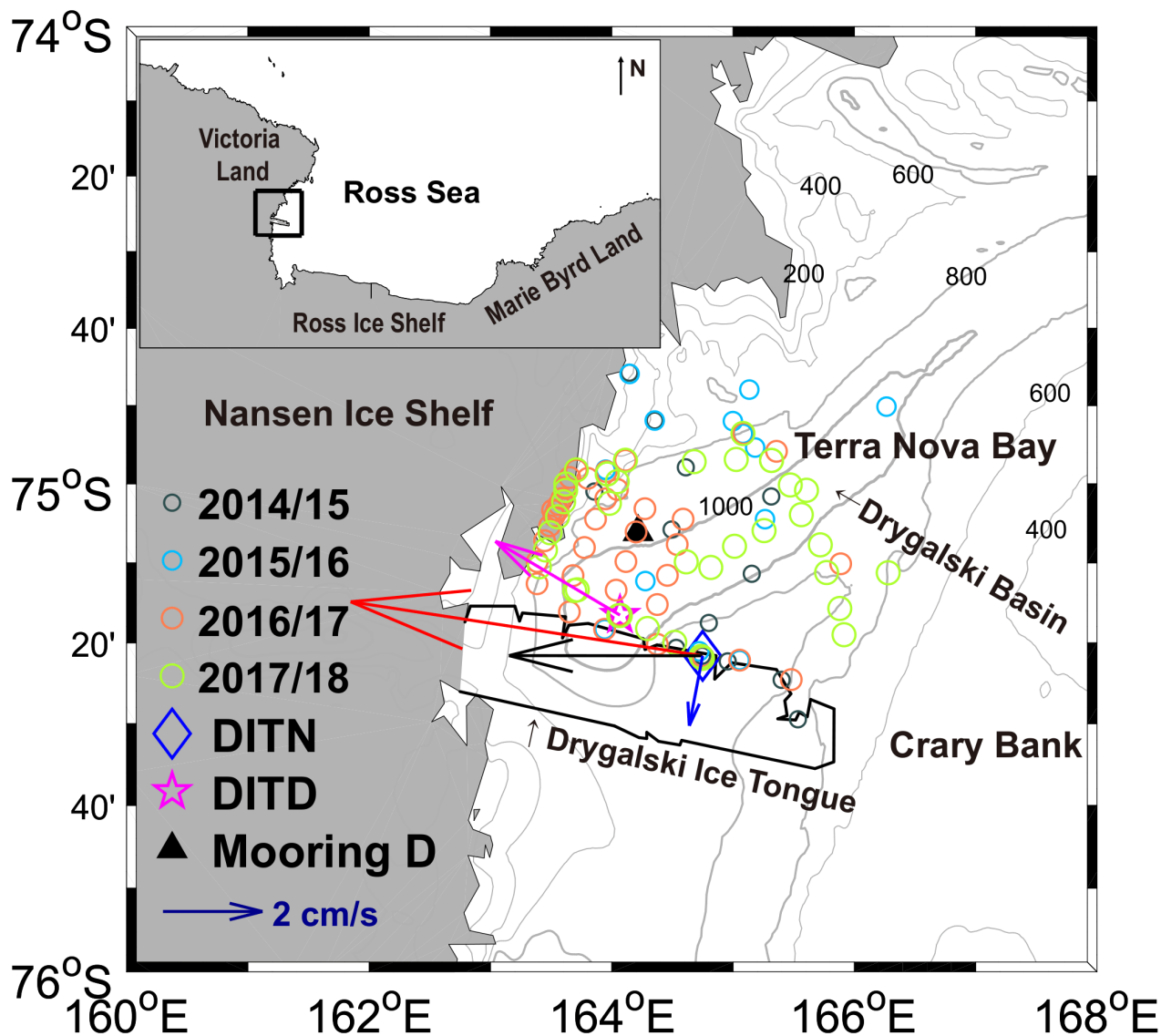
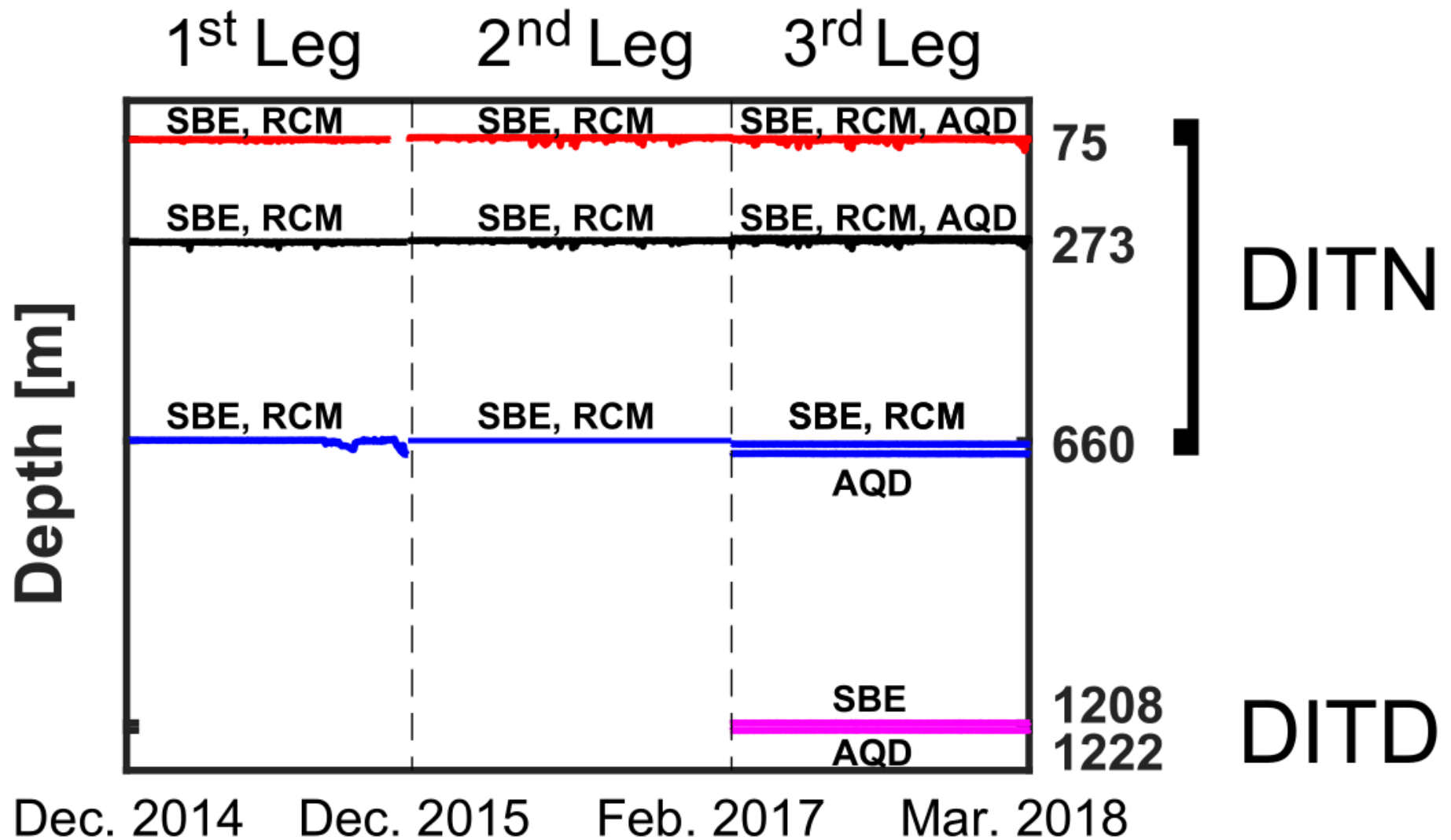


Figure 1: A topographic map of Terra Nova Bay (TNB). The location of TNB in the Ross Sea is shown in the upper-left inset. The bold grey line indicates the 1000-m isobaths and the interval between the thinner grey lines is 200 m. Conductivity-temperature-depth (CTD) stations in the austral summers (i.e., 2014, 2015, 2017, and 2018) are denoted by open circles. The averaged current vector from August to November at 660 m in the DITN (1222 m in the DITD) is denoted by a blue (magenta) arrow. The red (black) arrow indicates the mean current vector from June to November at 75 (273 m) in the DITN. The blue arrow in the bottom left indicates the reference velocity (2 cm s^{-1}).



510 **Figure 2:** The recorded sensor depths during the three observation legs. The red, black, and blue lines show the depth time series for sensors at the upper-, mid-, and deep-layer of the DITN. A magenta line also shows the recorded sensor depths of the DITD. The SBE, RCM, and AQD represent the SBE37SM, RCM9, and Aquadopp current meters, respectively (see details in Table 1).

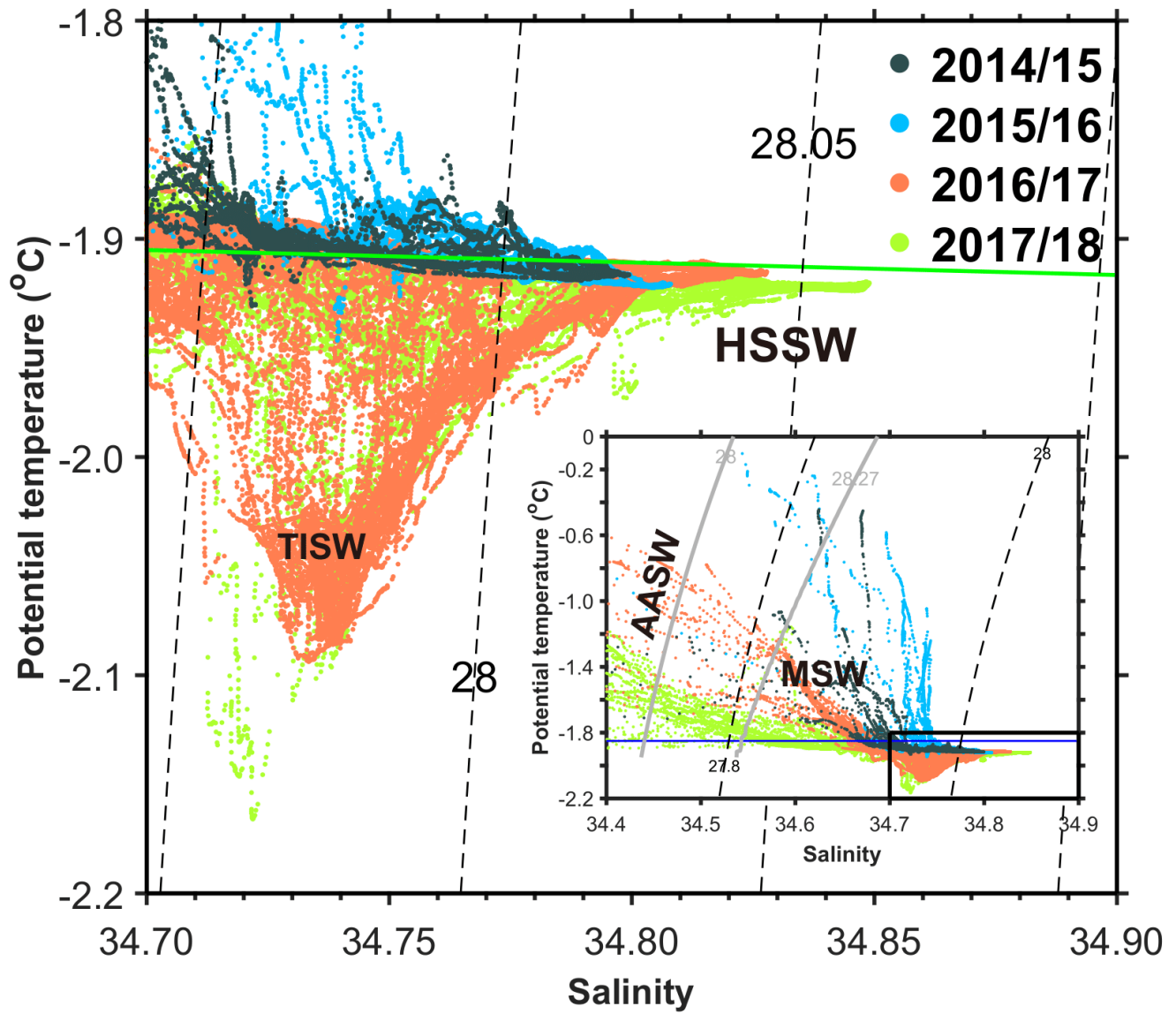


Figure 3: A zoomed-in plot of the θ -S (potential temperature-salinity) diagram for CTD data observed in TNB during each observation period. The green solid line denotes the freezing point at the surface depending on salinity, and the black dashed lines indicate isopycnals. The full range θ -S diagram is shown in the small lower-right inset. The black box and blue line indicate the ranges of the magnified plot, and the -1.85 °C isotherm, respectively. The grey solid lines denote 28 and 28.27 kg m^{-3} neutral density (γ^n) surfaces. AASW, MSW, TISW, and HSSW represent the Antarctic Surface Water, Modified Shelf Water, Terra Nova Bay Ice Shelf Water, and High-Salinity Shelf Water, respectively.

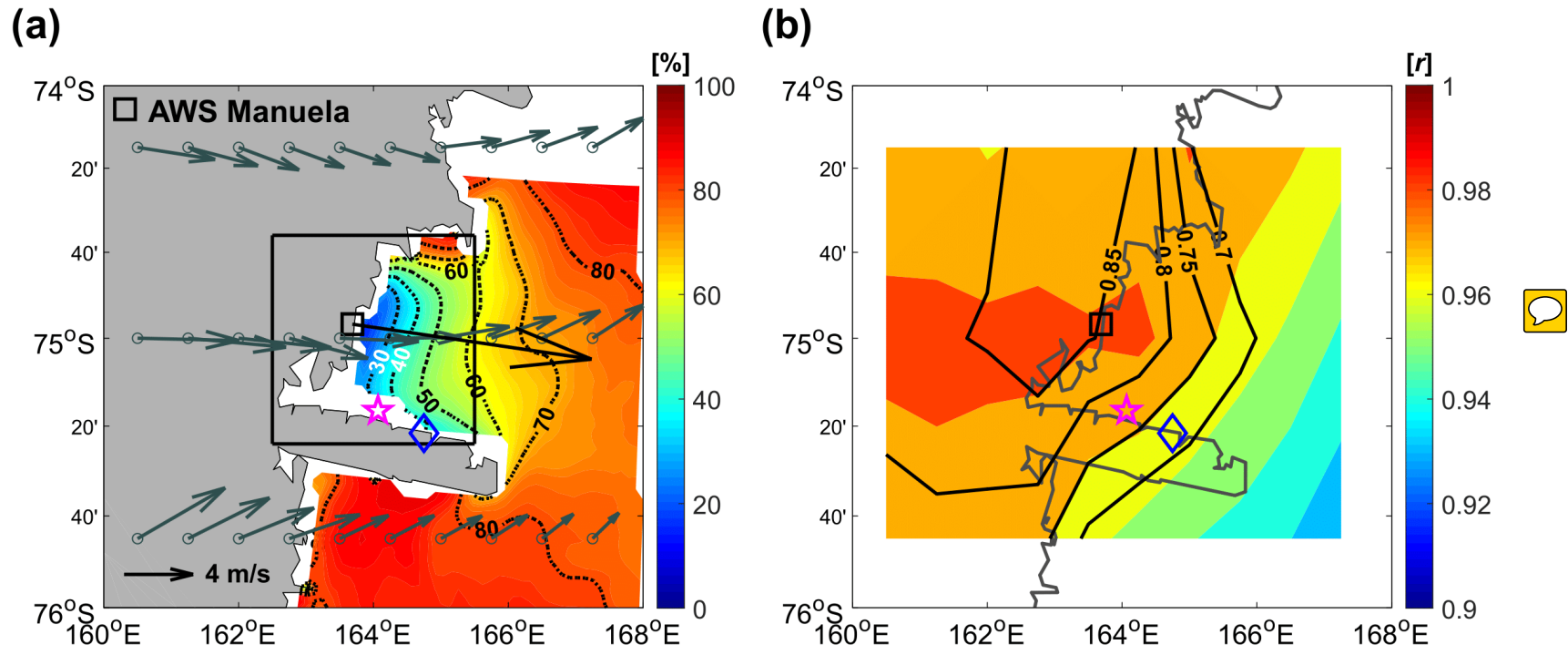


Figure 4: (a) Spatial distributions of averaged sea-ice concentrations from July 2014 to March 2018. The interval of the dotted contour lines is a concentration of 10%. The black square (blue diamond and magenta star) indicates the Automatic Weather System (AWS) Manuela station (DITN and DITD). The dark-grey (black) arrow is a mean wind vector for July 2014–March 2018 using ERA-Interim data (data from AWS Manuela station). The black box denotes an averaged region for sea ice concentrations. (b) Spatial distributions of the correlation coefficients (r) between daily air temperature for ERA-Interim and Manuela during July 2014–March 2018. The black solid contour lines indicate the horizontal distributions of r between daily eastward wind speed from ERA-Interim and Manuela during the same period.

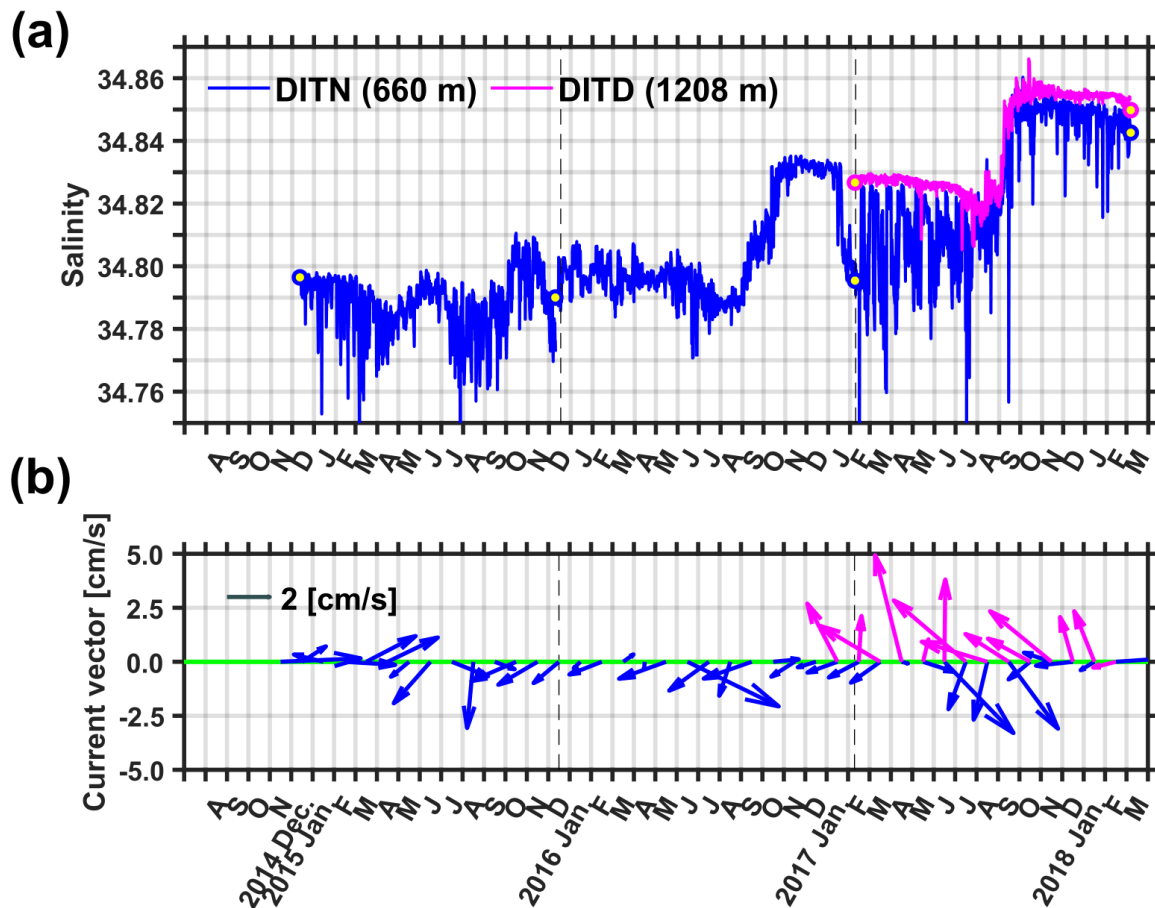


Figure 5: (a) Time series of deep salinity observed in the DITN (blue) and DITD (magenta) from December 2014 to March 2018. The blue (magenta) circles filled with yellow indicate the averaged salinity in a 5-m layer at the bottom obtained using CTD data observed near the DITN (DITD). The black dashed line divides periods of each leg in the moorings (see details in Table. 1). (b) Monthly mean current vectors at 660 m in the DITN and 1222 m in the DITD are indicated by blue and magenta arrows.

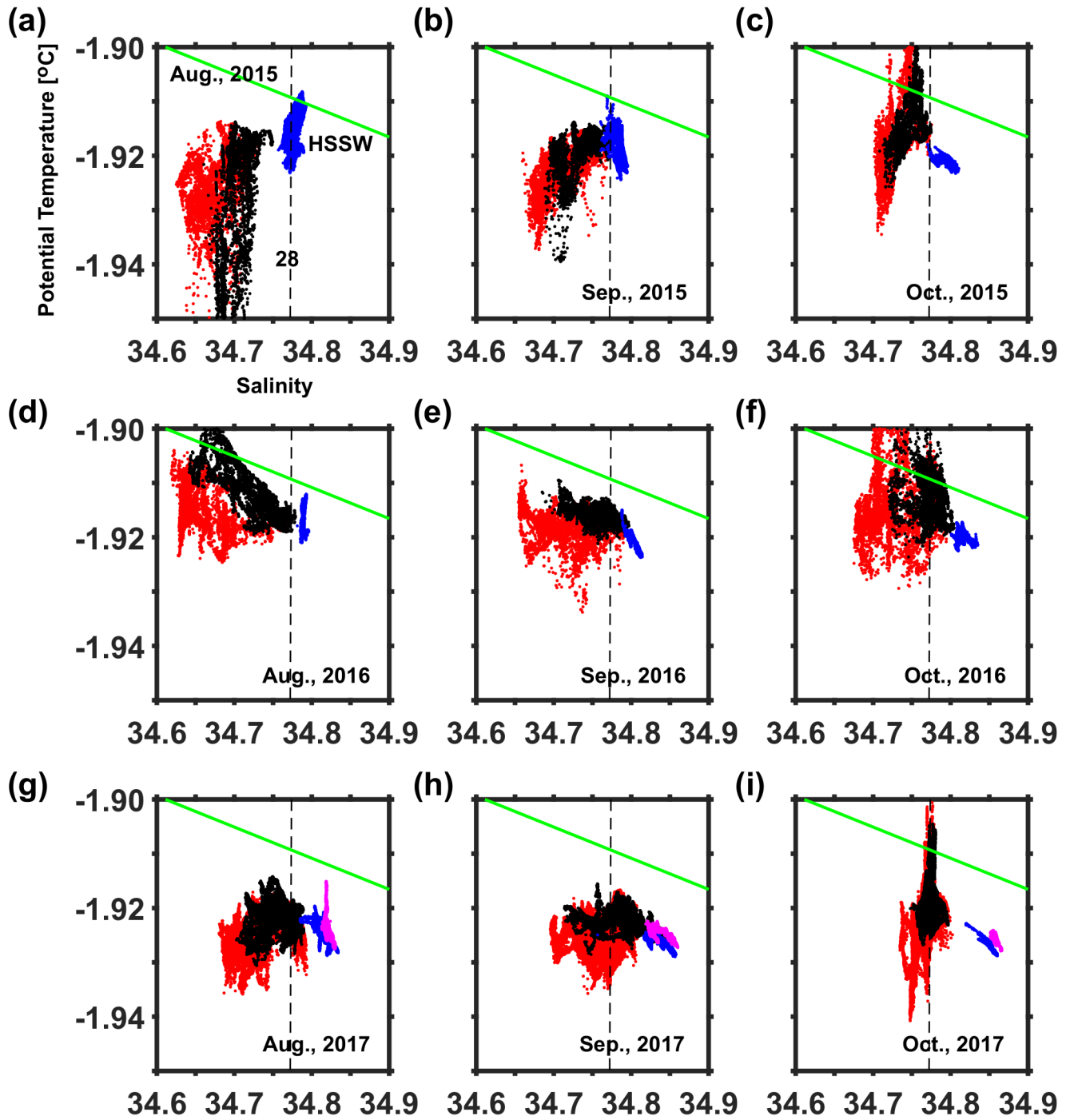


Figure 6: (a) A magnified version of the θ -S (potential temperature-salinity) diagram for data from the DITN and DITD in August 2015. Red, black, and blue dots are θ -S at 75, 273, and 660 m, respectively. The green thin line denotes the freezing point at the surface depending on the salinity while the black dashed line indicates $\sigma_\theta = 28.00 \text{ kg m}^{-3}$. (b) The same as Fig. 6a, but for September 2015. (c) The same as Fig. 6a, but for October 2015. (d–f) The same as Fig. 6a–6c, but for August–October 2016. (g–i) The same as Fig. 6a–6c, but for August–October 2017. Magenta dots are θ -S at 1208 m.

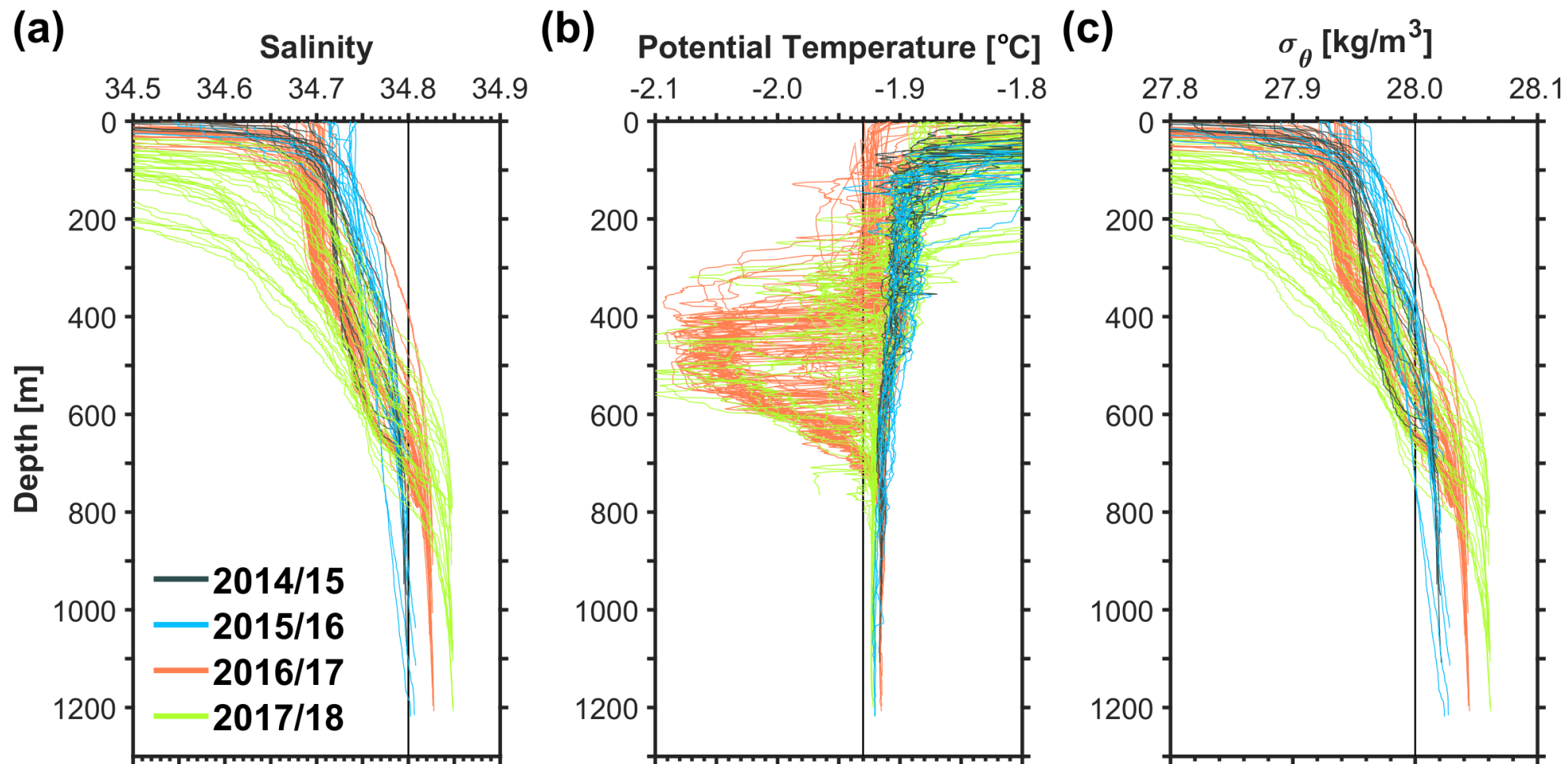


Figure 7: (a) Vertical salinity profiles at each observation period. The black solid line indicates 34.8 (b) The same as Fig. 7a, but for potential temperature, where the black solid line denotes -1.93°C . (c) The same as Fig. 7a, but for potential density (σ_θ), where the black solid line indicates 28.0 kg m^{-3}

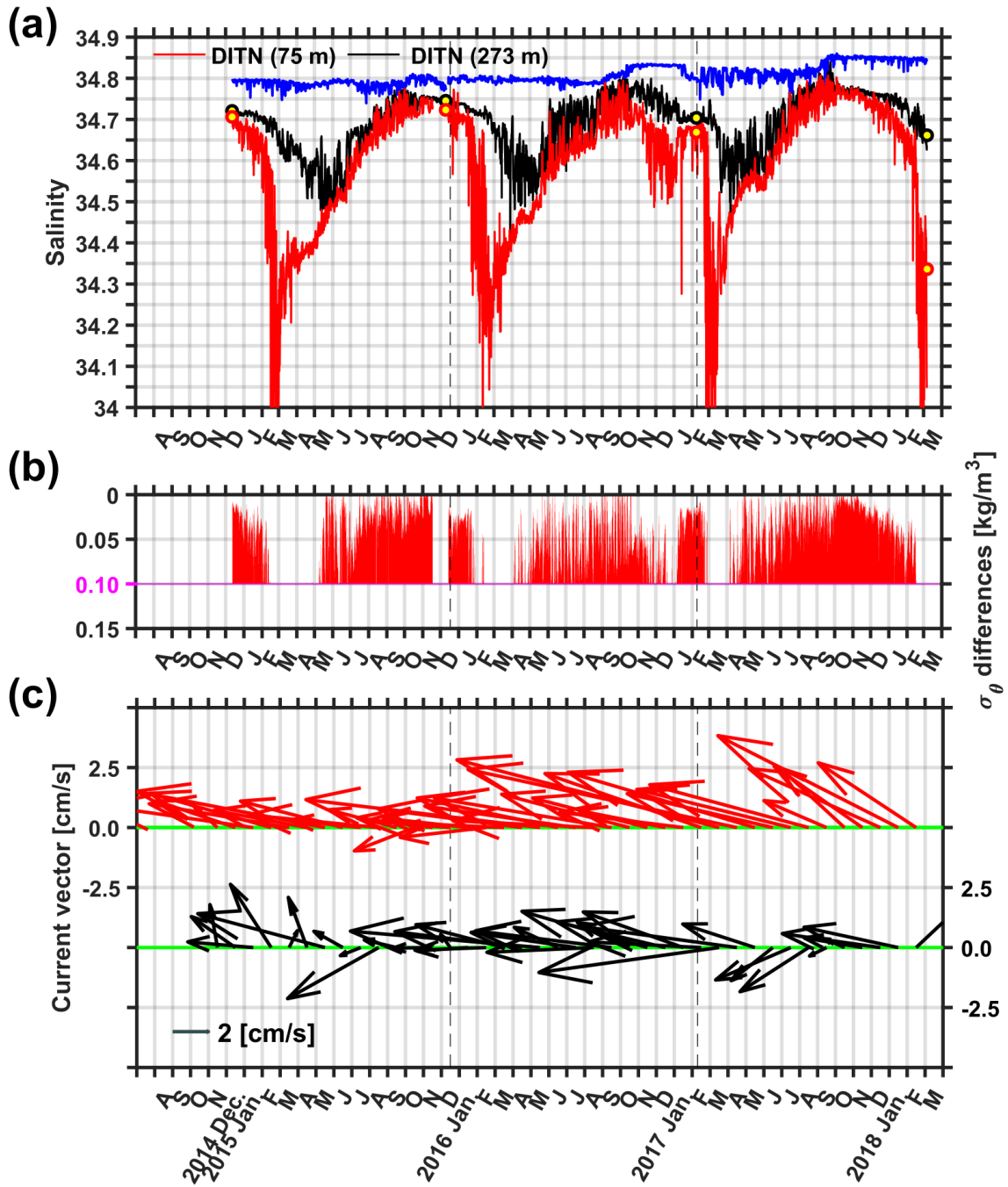


Figure 8: (a) Salinity time-series at three depths from the DITN. The red (black) circles filled with yellow are the averaged salinity in a 5-m layer at 75 (273) m obtained using CTD data observed near the DITN. The black dashed line divides periods of each leg at the moorings (see details in Table. 1). (b) Potential density (σ_θ) differences lower than 0.10 kg m⁻³ for σ_θ at 75 and 273 m. The magenta line indicates a 0.10 kg m⁻³ difference. (c) Monthly mean current vectors at 75 and 273 m of the DITN are indicated by red and black arrows.

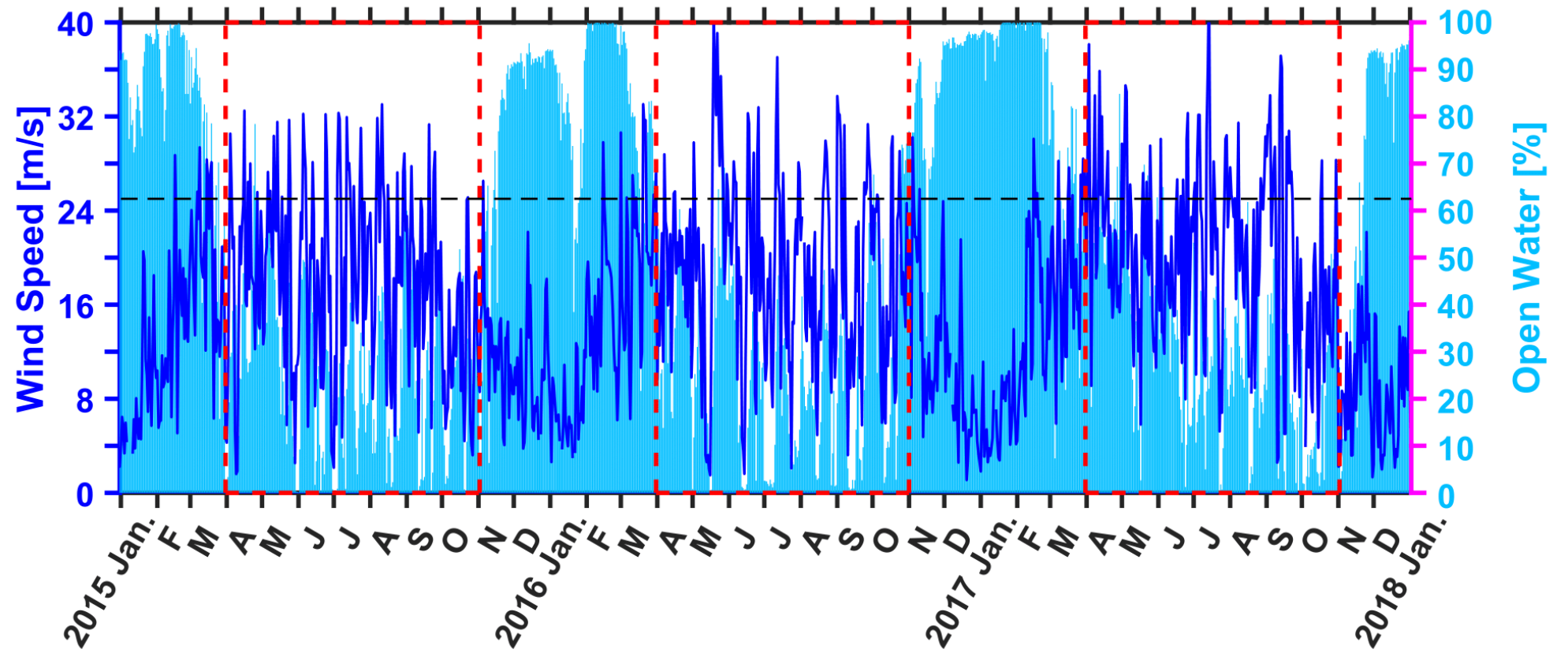


Figure 9: Time-series from 2015 to 2017 for daily eastward ($225^\circ < \theta < 315^\circ$) wind speed from Manuela (blue line), as well as the daily percentage of open water averaged from the black box shown in Fig. 4a (sky blue bar). Red dashed boxes indicate a time domain from April to October. The black dashed line indicates a wind speed of 25 m s^{-1} .

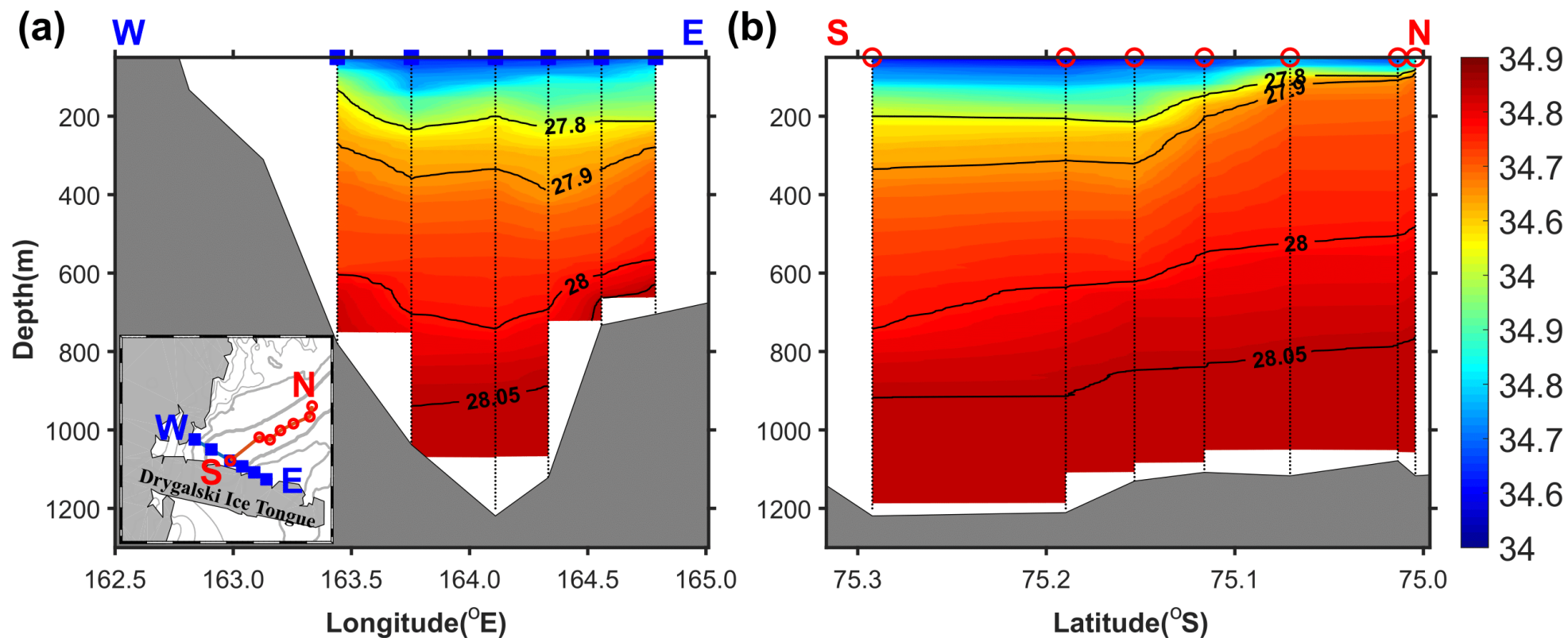


Figure 10: (a) Vertical section of salinity along the Drygalski Ice Tongue (blue-filled squares in the inset) observed during the 2017/18 survey. The colorbar for salinity is denoted in Fig. 10b and its interval is 0.01. The black contour lines indicate isopycnals (kg m^{-3}). (b) The same as Fig. 10a, but for the section along the Drygalski Basin (red circles in the inset of Fig. 10a).

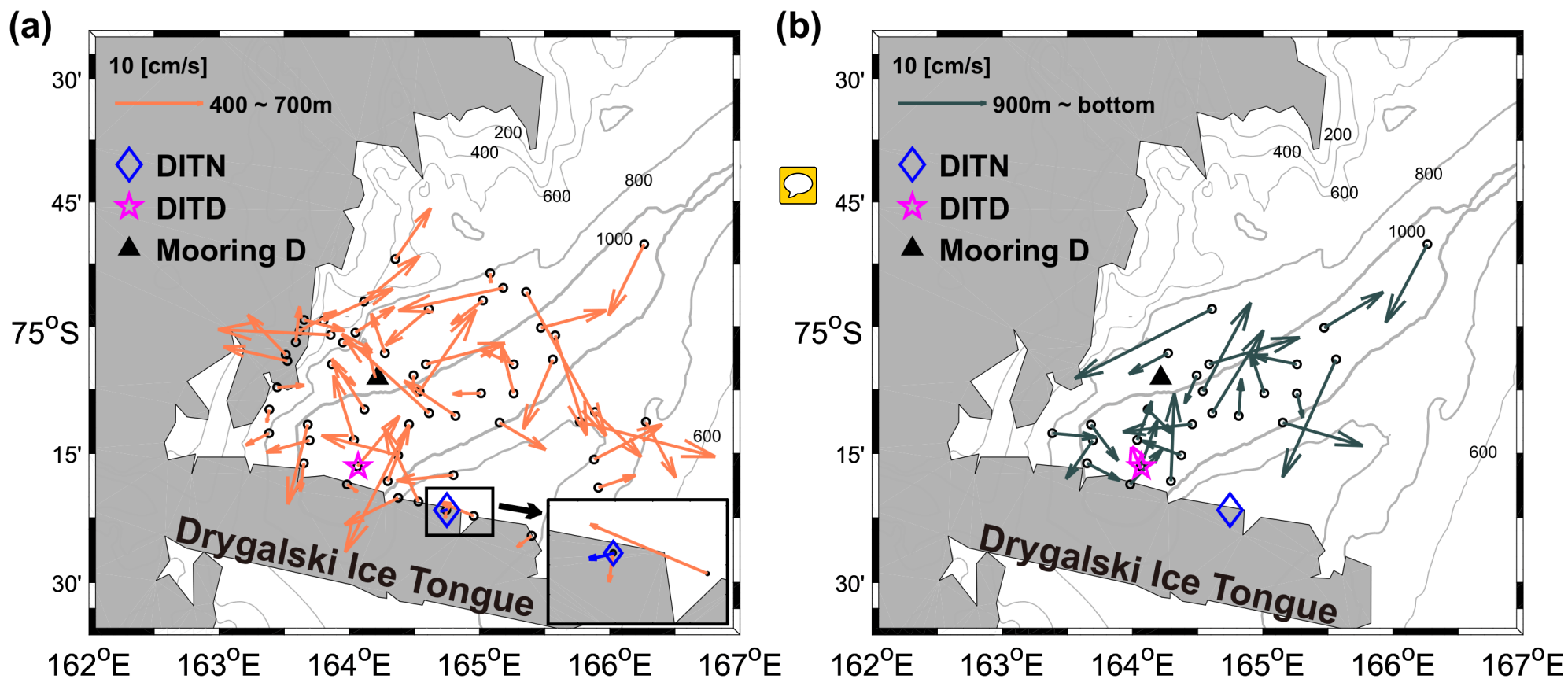


Figure 11: (a) Mean currents in a range of 400–700 m during four hydrographic surveys (see details in Table 1). The LADCP data from adjacent stations (< 3 km) are spatially averaged. The black circles denote the LADCP stations. The averaged current vector from January to February at 660 m in the DITN is denoted by a blue arrow. The inset shows the current vectors near the DITN. (b) The same as Fig. 11a, but for the range of 900 m–bottom. A magenta arrow shows the averaged current vector from January to February at 1,222 m in the DITD.

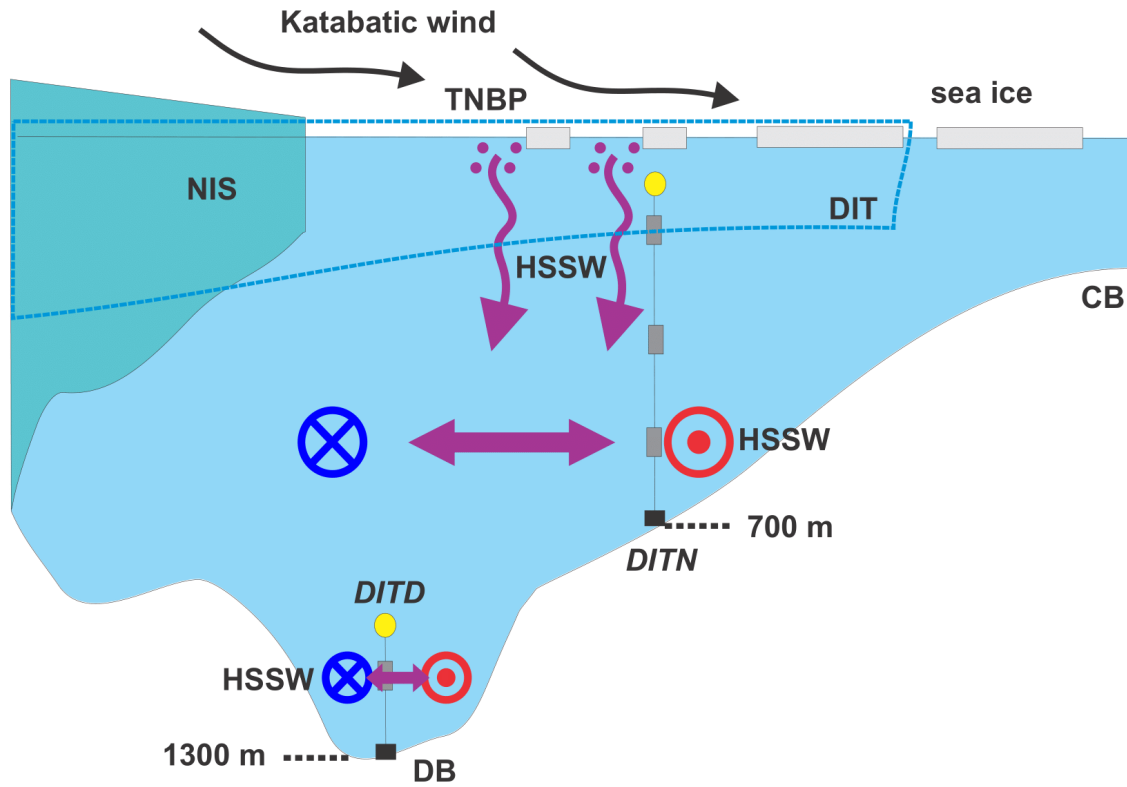


Figure 12: A schematic of the spatio-temporal variations in the production of HSSW in TNBP. The downward arrows show HSSW formation through convection led by a supply of brine from the surface, which is related to polynya development via winds. The brine rejecting process associated with sea-ice formation, which is driven by katabatic winds, is denoted with dots near the surface. The horizontal bi-directional arrows indicate that the HSSW that formed near the Nansen Ice Shelf (NIS) advects at the deepest depths of both eastern Terra Nova Bay (DITN) and Drygalski Basin (DITD) via cyclonic pattern flows in TNBP. The blue (red) circle represents outgoing (incoming) flow. DB, CB and DIT denote the Drygalski Basin, Crary Bank and Drygalski Ice Tongue, respectively.

Table 1. Information from the four oceanographic surveys and data observed from the DITN and DITD. U, V, T, C, and P represent the east-west current speed, north-south current speed, temperature, conductivity, and pressure, respectively. S, R, and A are the instrument abbreviations for the SBE37SM, RCM9, and Aquadopp current meters, respectively.

Survey	Period	Observation	Number of stations in TNB	Ave. Salinity (\pm std) in a 10-m layer at 900-m depth
2014/15	Dec. 11–16, 2014	Full-depth CTD/LADCP cast	11	34.796 (\pm 0.001)
2015/16	Dec. 8–15, 2015	Full-depth CTD/LADCP cast	10	34.791 (\pm 0.007)
2016/17	Jan. 26–Feb. 15, 2017	Full-depth CTD/LADCP cast	37	34.822 (\pm 0.002)
2017/18	Mar. 4–13, 2018	Full-depth CTD/LADCP cast	38	34.838 (\pm 0.005)
DITN	Period	Position	Depth [m]	Variables
1 st leg	Dec. 12, 2014–	75° 21' 37" S,	75 (S, R)	S: 10 min T, C, P R: 30 min U, V
	Dec. 10, 2015	164° 44' 58" E	275 (S, R)	
		(Depth: 675 m)	660 (S, R)	
2 nd leg	Dec. 12, 2015–	75° 21' 36" S,	72 (S, R)	S: 10 min T, C, P R: 60 min U, V
	Feb. 08, 2017	164° 44' 55" E	272 (S, R)	
		(Depth: 675 m)	660 (S, R)	
3 rd leg	Feb. 09, 2017–	75° 21' 39" S,	74 (S, R, A)	S: 2 min T, C, P R: 60 min U, V A: 15 min T, P, U, V
	Mar. 06, 2018	164° 44' 47" E	272 (S, R, A)	
		(Depth: 680 m)	665 (S, R, A)	
DITD	Period	Position	Depth [m]	Variables
3 rd leg	Feb. 08, 2017–	75° 16' 33" S,	1208 (S)	S: 2 min T, C, P A: 15 min T, P, U, V
	Mar. 06, 2018	164° 04' 02" E	1222 (A)	
		(Depth: 1230 m)		